
Article:
Cheng, F., Watton, P.N. orcid.org/0000-0002-5531-5953, Kurobe, M. et al. (4 more authors) (Submitted: 2021) A mechanobiological model of the urinary bladder : integrative modelling of outlet obstruction. Journal of the Mechanical Behavior of Biomedical Materials. ISSN 1751-6161 (Submitted)

A mechanobiological model of the urinary bladder: integrative modelling of outlet obstruction

Fangzhou Cheng[a], Paul N. Watton[a,d,1], Masahiro Kurobe[b], Ei-ichiro Takaoka[b], Chris Chapple[c], Naoki Yoshimura[b], Anne M. Robertson[a]

[a]*Department of Mechanical Engineering and Materials Science, University of Pittsburgh, Pittsburgh,United States*
[b]*Department of Urology, University of Pittsburgh, Pittsburgh, United States*
[c]*Sheffield Teaching Hospitals NHS Foundation Trust, Sheffield, United Kingdom*
[d]*Department of Computer Science & Insigneo Institute for in silico Medicine, University of Sheffield, Sheffield, United Kingdom*

Abstract

We present the first model to simulate the adaptive growth and remodeling (G&R) response of the bladder wall to bladder outlet obstruction (BOO). The model is calibrated and validated with an experimental rodent model of BOO. The bladder is modeled as a multi-layered, nonlinear elastic spherical membrane using a constrained mixture model that includes both passive and active components. The mechanical model is integrated with a shorter time scale micturition model that accounts for the active mechanics of voiding and dependence of flowrate on urethral resistance. Over a second time scale, constituents are configured and subsequently remodel to achieve a homeostatic state at the onset of voiding. Simulations of remodeling in response to the tenfold increase in outlet resistance arising from BOO, predict an initial loss of voiding capacity. Subsequent smooth muscle cell (SMC) hypertrophy enables the bladder wall to generate sufficient active tension to restore

[1]P.Watton@sheffield.ac.uk

voiding functionality. Consistent with the experimental observations, the model predicts: hypertrophy of SMC and enlargement of the bladder over realistic timescales; collagen remodeling to maintain its role as a protective sheath; and increased voiding duration with lower average flow rate. This integrative G&R modeling approach provides fundamental insight into the adaptation of the bladder's structural-functional relationship in response to outlet obstruction.
Keywords: bladder, growth, remodelling, biomechanics, mechanobiology

1. Introduction

The function of the bladder is to serve as a low pressure reservoir for storing urine and then efficiently expel this urine at a convenient time. Bladder outlet obstruction (BOO) is a urodynamic diagnosis that signifies the existence of increased urethral resistance, sufficient to alter the voiding process. Over time, BOO can lead to changes in the bladder's storage capacity as well. A clinical diagnosis of BOO is based on the presence of specific changes to the bladder pressure flow relationship that are defined in the International Continence Society (ICS) Standardisation report and can be measured using urodynamic studies [1]. The mechanical causes of BOO include an enlarged prostate, such as induced by benign prostatic hyperplasia (BPH) [2, 3, 4] and urethral narrowing from scarring or strictures [5, 6, 7]. BPH induced BOO is increasingly prevalent for men over the age of 50, with 50 - 75% of men over age 50 and 80% of men over age 70 experiencing lower urinary tract symptoms (LUTS) as a result of BPH[8], voiding hesitancy, prolonged micturition, incomplete bladder emptying, increased urination frequency, ur-

gency, and incontinence, which dramatically lower the quality of life, both physically and psychologically [9]. Two-thirds or more of the men with BOO have storage problems where there is increased urinary frequency associated with urgency to void, and the majority of these patients have bladder overactivity that is measurable in urodynamic testing [10]. The economic burden of BPH induced BOO is significant; 4 billion dollars annually in 2006, a sum that will only increase as the US population continues to age [11].

The structure of the bladder wall is often considered with respect to three layers: the mucosa, the muscularis propria (herein referred to as the detrusor smooth muscle (DSM) layer) and the adventitia. The mucosa is the innermost layer and is composed of an urothelium, a basement membrane and a lamina propria (LP) which contains a densely packed, interwoven network of collagen fibers. The DSM is a composite of smooth muscle cell (SMC) bundles intermixed with collagen and elastin fibers and the outer surface of the bladder is formed of loose connective tissue commonly termed the adventitia. During filling, the unfolding of the tissue layers allow the bladder to expand under low pressure[12]. To void, the contraction of the muscle cells is triggered to generate active stress and initiate flow by overcoming the urethral resistance.

In silico models of the bladder that have been developed to date can, broadly speaking, be classified into two main types: constitutive models [13, 14, 15, 16, 17, 18, 19, 12, 20, 21] and whole bladder micturition models [22, 23, 24, 25, 26, 27]. The constitutive models focus on the strain-stress relation for

the passive and, in some cases, active mechanical response, whilst the micturition models focus on simulating the pressure-flow relation of the bladder during voiding.

The bladder, like other soft tissues can alter its constituents and geometry through a growth and remodeling process. Recently, we developed an integrated constitutive model that combines a constrained-mixture model of this G&R process for the bladder wall with a micturition model[28]. Using this model, urodynamic curves can be interpreted with respect to the underlying microstructure (and vice-versa), providing fundamental insight into the structure-function relation of the bladder during filling and voiding. This coupled micturition/GR model has the potential to provide insights into bladder pathophysiology and its effect on bladder function. In the present work, we extend this model to the BOO bladder.

In bladders with BOO, the urethral resistance increases, requiring the SMC in the wall to generate larger pressures to void, inducing a growth and remodeling (G&R) response that leads to changes in bladder size and tissue composition [29]. While this G&R response can restore voiding, there can be associated deficits in mechanical function such as weak stream, incomplete emptying, and increased voiding frequency. The changes to bladder functionality are intimately related to changes in the mechanics and microstructure of the tissue. Although experimental and computational models of the G&R process, can potentially provide insight into the evolving pathophysiology of the BOO bladder, thus far, no computational models have been developed

to simulate the G&R evolution of any bladder disease.

In the present work, we extend Cheng et al. [28] model to incorporate G&R scheme and apply the model to simulate the adaptive response of the bladder to BOO. An integrative interdisciplinary modelling approach is adopted in which an experimental rat model of outlet obstruction is used to inform the *in silico* model. The model is parameterized using data from a healthy rat bladder, BOO is simulated by an increase in outlet resistance and competing hypotheses for the adaptive response of the bladder to increased urethral flow resistance are investigated.

The structure of the paper is as follows: Section 2 details the experimental model, protocols for tissue characterization and computational methodology; Section 3 illustrates model simulations and compares predictions with experimental observations. Lastly, Section 4 concludes with a summary and critique of the model and provides an outlook for future research.

2. Methods

We utilise an integrative *in vivo in-vitro in-silico* modelling approach (see Fig. 1). An *in silico* model is developed that simulates the mechanics of the micturition cycle in healthy bladder and it's G&R in response to outlet obstruction. Where possible, model parameters are informed from *in vivo* pressure-flow experiments and *in vitro* planar biaxial testing coupled with multi-photon microscopy of the collagen fibers.

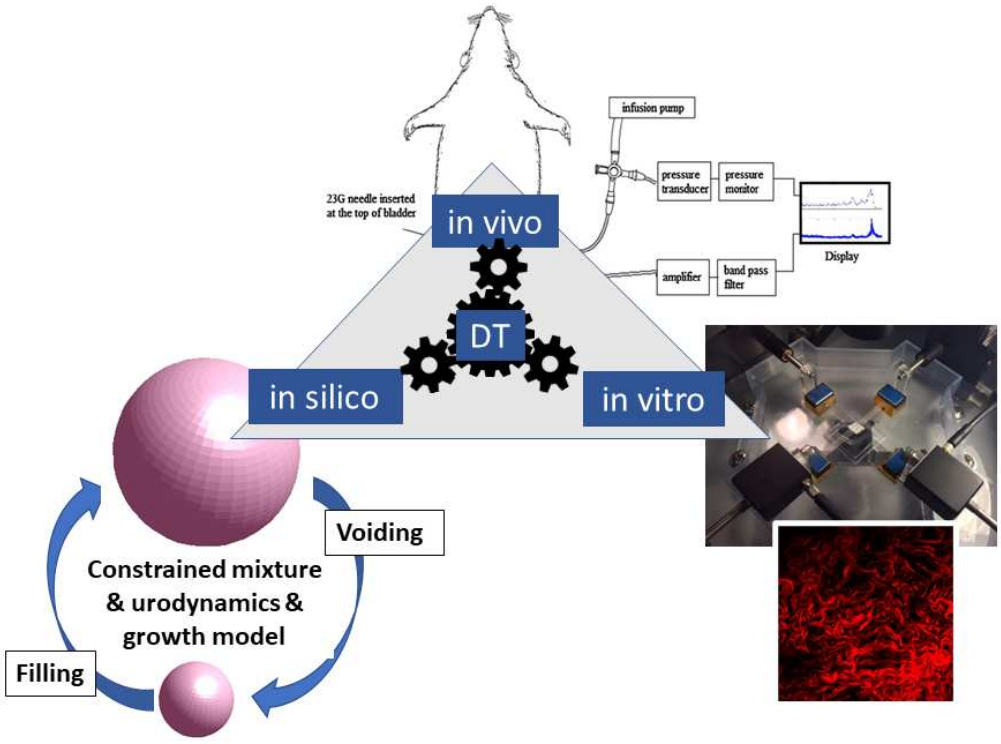

Figure 1: An integrative *in vivo in-vitro in-silico* modelling approach.

2.1. Experimental Studies of BOO Model

2.1.1. Creation of BOO model

Male Sprague Dawley rats were used for producing the experimental BOO model [30]. Briefly, under isoflurane anesthesia, the bladder and the proximal urethra were exposed via a lower abdominal midline incision. A 4-0 silk ligature was placed around the urethra and tied at the urethrovesical junction level proximal to the urethral fenestration with a metal rod (outside catheter diameter of 1.27 mm) placed alongside the urethra, and then the rod was removed. The abdominal wound was closed. This ligation was maintained in place throughout the duration of the experiments. Sham rats underwent similar procedures without urethral ligation.

2.1.2. In vivo measurements: pressure-flow study

Twenty four Sprague Dawley rats (twelve BOO and twelve SHAM) were used in the cystometry (pressure-flow) studies, performed 4 weeks after inducing BOO,[30]. Under isoflurane anaesthesia, a PE-50 polyethylene catheter (Clay-Adams, Parsippany, NJ) was inserted through the bladder dome and a purse-string suture was placed tightly around the catheter. The implanted catheter was exteriorized through the abdominal wall, and the wound was closed with 4-0 silk sutures. After the surgery, the rats were placed in restraining cages (W 80 mm $\times$ L 300 mm $\times$ H 150 mm, Yamanaka Chemical Ind., Ltd, Osaka, Japan) and allowed to recover from isoflurane anaesthesia for 1–2 h before starting cystometry. After recovery, a three-way stopcock was used to connect the intravesical catheter to a pressure transducer (Transbridge 4M, World Precision Instruments, Sarasota, FL, USA) for recording intravesical bladder pressure and to a syringe pump (*company*) for infusing

saline at a fixed flowrate. Because variability in bladder capacity among BOO rats is typical of this model, saline was initially infused at 0.1 ml/min; subsequently, the infusion rate was adjusted to 0.04–0.3 ml/min to obtain an intercontraction interval around 10-15 min [31]. Intravesical pressure changes were measured using data acquisition software (AD Instruments, Castle Hill, NSW, Australia) at a sampling rate of 100 Hz using a PowerLab. Saline infusion was continued until stable voiding cycles were established.

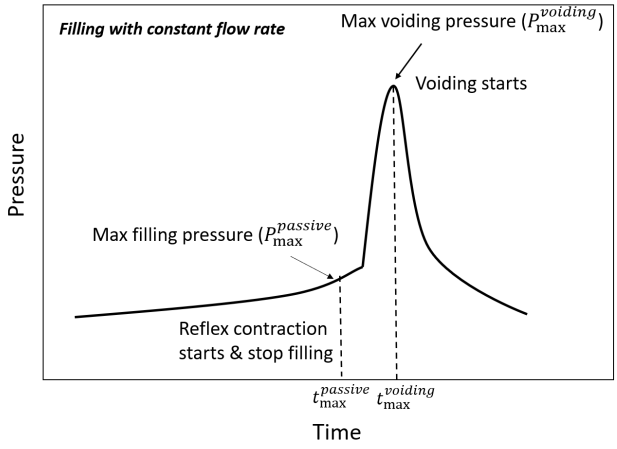

Figure 2: Schematic representation of the pressure flow curve during the cystometry study

The recorded data was used to construct the presssure/flow curves (Fig. 2), from which the following parameters were evaluated: (i) maximum voiding pressure $P_{max}^{voiding}$ (the peak pressure minus the basal pressure during each voiding cycle); (ii) maximum passive filling pressure $P_{max}^{passive}$ (the pressure immediately after the reflex contraction minus the basal pressure; the basal pressure is the the passive pressure in the empty bladder and measured from

Quantities	symbol	SHAM	BOO
void volume (ml)	V_{void}	0.84 $\pm$ 0.03	0.82 $\pm$ 0.12
residual volume (ml)	$V_{residual}$	0.02 $\pm$ 0.008	1.2 $\pm$ 0.23
void duration (s)	t_{void}	12 $\pm$ 0.4	45 $\pm$ 5
max filling pressure (Pa)	$P_{max}^{passive}$	300 $\pm$ 80	280 $\pm$ 70
max void pressure (Pa)	$P_{max}^{voiding}$	3900 $\pm$ 220	8900 $\pm$ 640

Table 1: In vivo measured parameters for SHAM and BOO experimental models.

the lowest pressure during cystometry). We define the maximum active voiding pressure (P_{max}^{active}) as the difference between maximum voiding pressure and maximum passive filling pressure, i.e. $P_{max}^{active} = P_{max}^{voiding} - P_{max}^{passive}$. Measured quantities are summarised in Table 1.

Voided urine was collected using a plastic cup placed underneath the restraining cage and measured to determine the voided volume (V_{void}), and post-void residual volume V_v was collected and measured by draining the post-void bladder using the bladder catheter with gravity [30]. Bladder capacity (V_F) was calculated as the sum of voided and residual volumes. After the bladder was harvested, the ex-vivo unloaded width (W_0), height (D_0) and thickness of the bladder were measured (see Tables. 2 and 3).

2.2. Constitutive Modeling for the Bladder Wall Mechanics

The bladder wall experiences large displacements that are modeled as quasi-static and constrained to be isochoric (as the bladder is idealized as incompressible). In the absence of external body forces, the displacement

Sham	S01	S02	S03	S04	Average	STD
unloaded width W_0 (mm)	4.31	5.05	4.76	4.84	4.74	0.27
unloaded height D_0 (mm)	11.10	10.32	9.64	9.36	10.10	0.67
unloaded thickness (mm)	0.72	0.71	0.85	0.82	0.78	0.06

Table 2: Dimensions of Sham bladders (n=4)

BOO	B01	B02	B03	B04	Average	STD
unloaded width W_O (mm)	7.92	8.40	9.38	10.08	8.95	0.84
unloaded height D_0 (mm)	19.14	17.39	13.75	15.35	16.41	2.04
unloaded thickness (mm)	1.61	1.53	1.98	1.10	1.56	0.36

Table 3: Dimensions of BOO bladders (n=4)

field therefore must satisfy the following equilibrium equation $\nabla \cdot \underline{\underline{\sigma}} = 0$ where $\underline{\underline{\sigma}}$ is the Cauchy stress tensor. We assume an additive decomposition of the stresses due to the passive and active components

$$\underline{\underline{\sigma}} = \underline{\underline{\sigma_p}} + \underline{\underline{\sigma_a}}. \tag{1}$$

2.2.1. Kinematics

The Lagrangian formulation used in this work denotes the deformation gradient as $\underline{\underline{F}}$, and the right Cauchy-Green tensor as $\underline{\underline{C}} = \underline{\underline{F}}^T \underline{\underline{F}}$. The tensor invariants are $I_1 = tr(\underline{\underline{C}})$, $I_2 = (tr(\underline{\underline{C}})^2 - tr(\underline{\underline{C}}^2))/2$ and $I_3 = det(\bar{C}) = 1$. The direction of the collagen fibers is denoted by the unit vector $\boldsymbol{a}_c^i$ where i ranges over number of orientations at a point within the tissue. The stretch λ_{4c}^i in the fibre direction is

$$\left(\lambda_{4c}^i\right)^2 = I_{4c}^i = \boldsymbol{a}_c^i \cdot \underline{\underline{C}} \boldsymbol{a}_c^i \tag{2}$$

i.e., associated with I^i_{4c}, a pseudo-invariant of $\underline{\underline{C}}$ and $\boldsymbol{a}^i$. Similarly, denoting the SMC direction by the unit vector $\boldsymbol{a}_m$, the stretch λ_{4m} in the SMC direction is

$$(\lambda_{4m})^2 = I_{4m} = \boldsymbol{a}_m \cdot \underline{\underline{C}} \boldsymbol{a}_m \tag{3}$$

2.2.2. Strain-energy functions

The strain energy function for the passive response of each layer L (where $L = LP$ denotes lamina propria, $L = DSM$ denotes the destrusor muscle layer and $L = ADV$ denotes the advential layer) receives contributions from elastin, passive smooth muscle cells and collagen fibers (anisotropic components). Hence

$$\Psi_L = \Psi_{L,e}(I_1) + \sum_i \Psi^i_{L,c}(I^i_{4c}). \tag{4}$$

Elastinous constitutents

The isotropic components are modeled as a neo-Hookean material [32]:

$$\Psi_{L,e} = K_{L,e}\left(I_1 - 3\right), \tag{5}$$

with $K_{L,e}$ being stiffness-like material constants.

Collagenous constituents

The constitutive model for the collagen accounts for the experimental observation that collagen fibers have a a distribution of waviness in the unloaded configuration and thus have a distribution of recruitment [33]. The strain energy function involves integrating the strain energy for a fiber ($\tilde{\Psi}^i_{L,c}$) over the distribution of recruitment stretches (ρ^i_{RL}),

$$\Psi_{L,c}(I^i_4) = m_{L,c} \cdot \sum_i \int_1^{\sqrt{I^i_4}} \tilde{\Psi}^i_{L,c}\left(\lambda^i_c\right) \rho^i_{RLc}\left(\lambda^i_{RLc}\right) d\lambda^i_{RLc}. \tag{6}$$

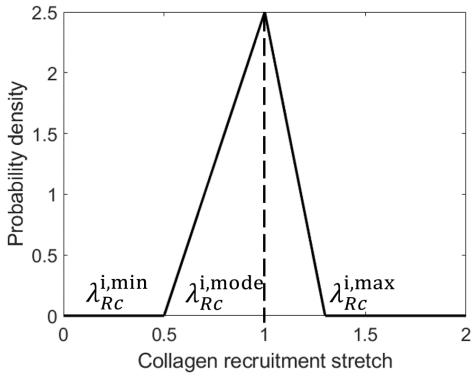

Figure 3: Schematic of triangular distribution of collagen recruitment stretch

where $m_{L,c}$ is the (dimensionless) normalized mass density of collagen fibers that can adapt to simulate collagen growth/atrophy[34]. We model each individual fiber to have a linear relationship between its 1st Piola-Kirchoff stress and its stretch (λ_c^i)([35, 36])

$$\tilde{\Psi}_{L,c}^i\left(\lambda_c^i\right) = \begin{cases} \dfrac{k_{L,c}^i}{2} \cdot \left(\lambda_c^i - 1\right)^2 & \lambda_c^i \geq 1 \\ 0, & \text{otherwise} \end{cases}, \tag{7}$$

where $K_{L,c}$ is a stiffness-like material constant and the fibre stretch λ_c^i is given by

$$\lambda_c^i = \frac{\lambda_{4c}^i}{\lambda_{RLc}^i} \tag{8}$$

$\lambda_{RLc}^i = \sqrt{I_{Rc}^i}$ denotes the recruitment stretch of the collagen fiber in layer L, and $\lambda_{4c}^i = \sqrt{I_{4c}^i}$.

The fiber recruitment distribution is represented with a triangular probability density function ρ_{Rc}^i [37, 35, 38, 36]; $\lambda_{Rc}^{i,q}$ relates to the the minimum ($q = min$), modal ($q = mode$) and maximum ($q = max$) recruitment

stretches of the distribution (see Fig. 3). More specifically:

$$\rho^i_{RL}\left(\lambda^i_{RLc}\right) = \begin{cases} 0, & \lambda^i_{RLc} \leq \lambda^{i,min}_{RLc} \\ g_1(\lambda^i_{RLc}), & \lambda^{i,min}_{RLc} < \lambda^i_{RLc} \leq \lambda^{i,mode}_{RLc} \\ g_2(\lambda^i_{RLc}), & \lambda^{i,mode}_{RLc} < \lambda^i_{RLc} \leq \lambda^{i,max}_{RLc} \\ 0, & \lambda^{i,max}_{RLc} < \lambda^i_{RLc}, \end{cases} \tag{9}$$

where

$$\begin{aligned} g_1(\lambda^i_{RLc}) &= \frac{2\left(\lambda^i_{RLc} - \lambda^{i,min}_{RLc}\right)}{\left(\lambda^{i,max}_{RLc} - \lambda^{i,min}_{RLc}\right)\left(\lambda^{i,mode}_{Rc} - \lambda^{i,min}_{RLc}\right)} \\ g_2(\lambda^i_{RLc}) &= \frac{2\left(\lambda^{i,max}_{RLc} - \lambda^i_{4RLc}\right)}{\left(\lambda^{i,max}_{RLc} - \lambda^{i,min}_{RLc}\right)\left(\lambda^{i,max}_{RLc} - \lambda^{i,mode}_{RLc}\right)}. \end{aligned} \tag{10}$$

Insertion of equations 12 and 9 into 6 and integration yields analytic expressions for the strain energy from which analytic expressions for the collagen stress can be derived (see [36]). The three main parameters of the distribution ($\lambda^{i,min}_{Rc}$, $\lambda^{i,mode}_{Rc}$, $\lambda^{i,max}_{Rc}$) are inferred from collagen fibre attachment stretch distributions at the onset of voiding.

2.2.3. SMC active stress

The active stress generated by the bladder during voiding is correlated to nerve activity [39] and occurs over a large range of bladder contractility [40], i.e. the active stress is generated within a range of SMC stretch, λ^{min}_m to λ^{max}_m, and is zero outside this range. We define the active (Cauchy) stress, σ^{act}_m, to be a function of SMC stretch (λ_m), nervous stimuli $S(t)$ and normalised

SMC mass-density m_m, i.e. $\sigma_m^{act} = \sigma_m^{act}(S(t), m_m(\tau), \lambda_m(t))$.

$$\sigma_m^{act} = \begin{cases} S(t) m_m k_m^{act} (\lambda_m)^4 (\lambda_m - \lambda_m^{min})(\lambda_m^{max} - \lambda_m) & \lambda_m^{min} \leq \lambda_m \leq \lambda_m^{max} \\ 0 & \text{otherwise} \end{cases} \tag{11}$$

where the SMC stretch λ_m is related to the tissue stretch by

$$\lambda_m = \frac{\lambda_{4m}}{\lambda_{Rm}} \tag{12}$$

and λ_{Rm} is the SMC recruitment stretch. We set $\lambda_m^{min} = 0.25$ and $\lambda_m^{max} = 2.5$. Examples of SMC stretch and active pressure curves are shown in Fig. 13.

The stimuli $S(t)$ ramps up at the onset of voiding and incorporates a feedback mechanism to decrease the stimulus and when the flow rate falls below a critical value Q_{crit} ($Q_{crit} = 0.02ml/s$) at $t = t_{crit}$, i.e.

$$S(t) = \begin{cases} 1 - \frac{1}{1+(t/k_1)^4} & 0 \leq t \leq t_{crit} \\ \left(1 - \frac{1}{1+(t_{crit}/k_1)^4}\right)\left(\frac{1}{1+((t-t_{crit})/k_2)^4}\right) & t_{crit} < t \leq t_{end} \\ 0 & t > t_{end} \end{cases} \tag{13}$$

where $k_1 = 1$ and $k_2 = 2$ control the rate of increase and decrease of signal strength, respectively; t_{end} denotes when $Q(t) = 0$.

2.3. Micturition Model

Due to the induction of BOO, the pressure required to void the bladder increases. Initially, the SMCs cannot generate sufficient tension to achieve this pressure and urine only exits the bladder through leakage. As remodeling progresses, the SMC mass increases and the bladder recovers the capacity for

voiding. As elaborated on below, the micturition model of the BOO bladder therefore has two different states (see Fig.4): *active bladder* and *leaky bladder*. The animal model initially exhibited the early phase of leaky bladder shown by overflow incontinence due to BOO-induced high urethral resistance. Then, the active bladder phase with micturition events gradually developed along with SMC hypertrophy.

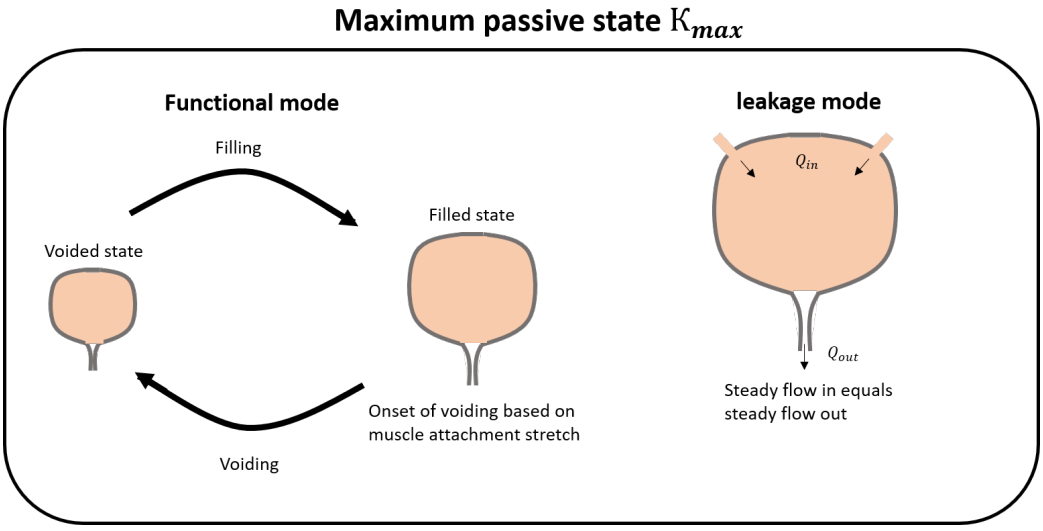

Figure 4: Schematic implication of the bladder maximum passive state under two different modes: functional mode (left) and leakage mode (right)

Active bladder. In the active bladder state, the SMCs are able to generate sufficient wall tension to overcome the urethral outlet resistance and induce voiding. For the *in silico* model, this process is simulated through a coupling between SMC stretch and the active stress generated by the SMCs. In particular, as the bladder fills and enlarges, the nervous stimulus function $S(t)$ is triggered when the SMC stretch reaches a critical value, i.e. when $(\lambda_m = \lambda_m^{at})$. Consequently, SMC active stress increases and voiding is initi-

ated when the internal bladder pressure (*passive + active*) exceeds the cutoff pressure (P_c) at which the urethra opens and closes. Voiding is complete when the internal pressure falls below the cutoff pressure.

The temporal dynamics of the pressure and outflow-rate of the active bladder can be computed during voiding. Following earlier works, we assume a linear relationship between voiding flow rate $Q(t)$ and bladder pressure $P(\lambda, t)$ [41, 42]:

$$Q(t) = \begin{cases} \frac{1}{\alpha}(P(\lambda,t) - P_c) & P(\lambda,t) > P_c \\ 0 & P(\lambda,t) \leq P_c \end{cases} \tag{14}$$

where α is the slope of the Pressure-Flow relationship and is a measure of urethral resistance. As voiding progresses, the updated volume is computed to calculate updated pressure ($P(\lambda, t)$). On completion of voiding, relevant metrics are calculated (volume voided, residual volume, voiding duration, contractile range).

Leaky bladder. If the bladder cannot generate sufficient active pressure to overcome the BOO cutoff pressure P_c^{BOO} then it will continue to fill. As it enlarges, the passive pressure increases; when passive pressure exceeds the cutoff pressure, the bladder will begin to leak. A new steady state occurs when the passive pressure increases until the leaky flow rate matches the filling rate of the bladder, i.e. $Q_{out} = Q_{in}$. The passive pressure (P^{leaky}) this occurs at can be determined from eqn.14:

$$P^{leaky} = \alpha Q_{in} + P_c^{BOO} \tag{15}$$

2.4. Homeostasis, Growth and Remodelling

2.4.1. Homeostasis

Collagen. Collagen recruitment distributions of SHAM and BOO tissue samples were quantified using biaxial mechanical testing and multiphoton microscopy. The distribution of collagen stretches at the onset of voiding is calculated from recruitment stretch distributions and the *in vivo* stretch at the onset of voiding, i.e. $\lambda|_{\kappa_{max}}^{sham}$, $\lambda|_{\kappa_{max}}^{boo}$.

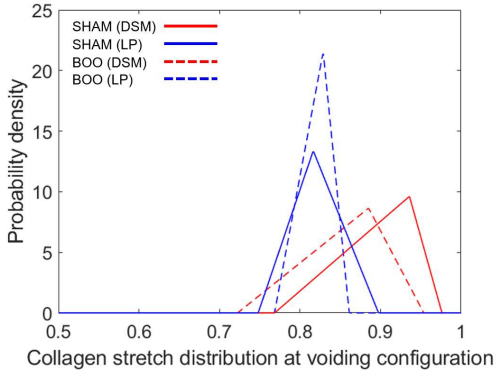

Figure 5: The average collagen stretch distribution at voiding configuration κ_V of BOO and SHAM

We observed that whilst the BOO bladder's onset of voiding radius increased by around 33%, collagen stretch distributions in this configuration were similar in each layer and maximum stretches were maintained below 1 (see Fig.5). Hence we observed that collagen is configured to be a protective sheath for the SHAM bladder and remodels during outlet obstruction to maintain this mechanical role. Based on our observations, for the *in silico* model, we assume that collagen is configured with a preferential stretch distribution at the onset of voiding and this distribution is fixed during re-

modelling; values for the distribution (see Table 4 are based based on Fig.5)

SMC. We assume SMC configures to achieve a preferred stretch at the onset of voiding, i.e. λ_m^{at}. We further assume that the muscle stretch at the onset of voiding is configured to the left of the maxima of the active pressure-muscle stretch curve which occurs at an SMC stretch of λ_m^{peak}, i.e.

$$\lambda_m^{at} = \lambda_m^{peak} - x \tag{16}$$

where we take $x = 0.1$. The rationale for this choice is as follows: configuring to the left of the peak still enables the bladder to generate active stress to void at a larger size (if voiding is withheld), Fig. 6; we don't configure too far to the left of the peak so that we can simulate a sufficient contractile voiding range.

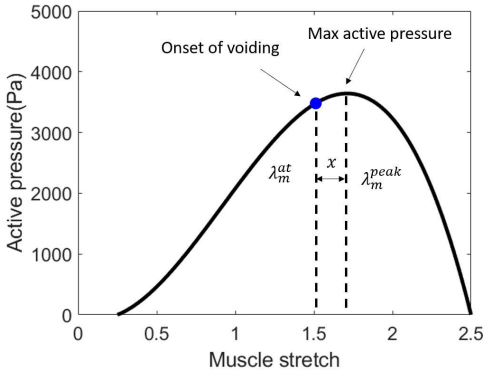

Figure 6: Schematic of muscle stretch vs. active pressure curve and configuration of muscle stretch at the onset of voiding

2.4.2. Remodelling

We assume that constituents are configured about the maximum passive state κ_{max} during the voiding cycle, i.e. about the onset of voiding for the *active bladder* and about the steady flow state for the *leaky bladder*.

Collagen. We assume collagen continually remodels to maintain it's mechanical role as a protective sheath at the maximum passive state (κ_{max}). Collagen recruitment stretch distributions remodel so that the collagen stretch distribution remodels towards the (homeostatic) attachment stretch distribution[35, 38, 36]:

$$\frac{\partial \lambda_{RLc}^{min}}{\partial \tau} = \alpha_c \frac{\lambda_{Lc}^{max}(\tau)|_{\kappa_{max}} - \lambda_{Lc}^{at,max}}{\lambda_{Lc}^{at,max}} \tag{17}$$

$$\frac{\partial \lambda_{RLc}^{mod}}{\partial \tau} = \alpha_c \frac{\lambda_{Lc}^{mod}(\tau)|_{\kappa_{max}} - \lambda_{Lc}^{at,mod}}{\lambda_{Lc}^{at,mod}} \tag{18}$$

$$\frac{\partial \lambda_{RLc}^{max}}{\partial \tau} = \alpha_c \frac{\lambda_{Lc}^{min}(\tau)|_{\kappa_{max}} - \lambda_{Lc}^{at,min}}{\lambda_{Lc}^{at,min}} \tag{19}$$

where the max, mode and minimum collagen fibre stretches evaluated at κ_{max} are, respectively:

$$\lambda_{Lc}^{max}|_{\kappa_{max}} = \frac{\lambda|_{\kappa_{max}}}{\lambda_{RLc}^{min}}, \qquad \lambda_{Lc}^{mod}|_{\kappa_{max}} = \frac{\lambda|_{\kappa_{max}}}{\lambda_{Rc}^{mod}}, \qquad \text{and} \qquad \lambda_{Lc}^{min}|_{\kappa_{max}} = \frac{\lambda|_{\kappa_{max}}}{\lambda_{RLc}^{max}}. \tag{20}$$

Muscle cells. We hypothesise that SMCs remodel to maintain their stretch towards a homeostatic value about the onset of voiding, i.e. typical maximum passive state, κ_{max}:

$$\frac{\partial \lambda_{Rm}}{\partial \tau} = \alpha_m \frac{\lambda_m(\tau)|_{\kappa_{max}} - \lambda_m^{at}|_{\kappa_{max}}}{\lambda_m^{at}} \tag{21}$$

Where λ_{Rm} is the SMC recruitment stretch, λ_m^{at} is the SMC attachment

stretch, α_m is a remodeling rate parameter and $\lambda_m|_{\kappa_{max}}$ is the SMC stretch at the maximum passive state, i.e. at the onset of voiding or leaky bladder.

2.4.3. Growth

The bladder responds to outlet obstruction with SMC hypertropy so that it can generate more force to overcome the outlet resistance and successfully void. In this study, we simulate SMC hypertrophy by evolving the SMC mass density and consider three illustrative mechanisms to drive growth. SMC hypertrophies to maintain: (i) volume voided; (ii) average voiding flow rate; (iii) contractile range.

Muscle growth driven by total voided volume. Based on the experimental observations, the total voided volume of bladder is restored at 4 weeks post-obstruction. Thus we assumed that the muscle grows to maintain the total volume voided of bladder.

$$\frac{\partial m_{smc}}{\partial \tau} = \beta_{smc} m_{smc} \left(\frac{V^0_{void} - V_{void}(\tau)}{V^0_{void}} \right) \tag{22}$$

where V^0_{void} is the volume voided at $\tau = 0$ (normal bladder) and $V_{void}(\tau)$ is the volume voided at time τ; β_{smc} is the growth rate parameter of muscle cells.

Muscle growth driven by average flow rate during voiding. The urethra can sense flow[43] and we assume that the the muscle grows was driven by the average flow rate of voiding sensed by urethra. Specifically,

$$\frac{\partial m_{smc}}{\partial \tau} = \beta_{smc} m_{smc} \left(\frac{Q^0_{avg} - Q_{avg}(\tau)}{Q^0_{avg}} \right) \tag{23}$$

Where $Q_{avg}(0)$ is the average voiding flow rate at $t = 0$ (normal bladder) and $Q_{avg}(\tau)$ is the average voiding flow rate at time τ.

Muscle growth driven by muscle contraction range during voiding. We assumed that the muscle grows to maintain the contraction range λ_{m-cyc} during voiding, which is defined as the difference between the muscle stretch at the filled state λ_m^F and the muscle stretch at the voided state λ_m^V, i.e.

$$\frac{\partial m_{smc}}{\partial \tau} = \beta_{smc} m_{smc} \left(\frac{\lambda^0_{m-cyc} - \lambda_{m-cyc}(\tau)}{\lambda^0_{m-cyc}} \right) \tag{24}$$

where $\lambda_{m-cyc} = \lambda_m^F - \lambda_m^V$ and, λ^0_{m-cyc} and $\lambda_{m-cyc}(\tau)$, are the muscle contractile ranges during voiding at $\tau = 0$ and τ, respectively.

Evolution of wall thickness. Hypertropy of SMC will lead to a thickening of the bladder wall. The evolving wall thickness can be inferred from initial constituent volume fractions and constituent mass-densities; this allows for comparison with experimental observations. For the geometrical model of the bladder considered (spherical membrane), the wall thickness in the voiding configuration, $h_g(t)$, is

$$h_g(t) = H_0 \hat{v}(t) \frac{1}{\lambda(t)^2 \mid_{\kappa_{max}}} \tag{25}$$

where $\lambda_{onset}(t)$ denotes the stretch at onset of voiding and the normalised tissue volume $\hat{v}(t)$ is

$$\hat{v}(t) = f_e^0 m_e(t) + f_c^0 m_c(t) + f_m^0 m_m(t), \tag{26}$$

and f_e^0, f_c^0, f_m^0 are initial volume fractions of elastin, collagen and SMCs. We assumed that at $t = 0$, the volume fractions of elastin, collagen, and SMCs are 10%, 30% and 60%, respectively.

2.5. Computational Implementation

2.5.1. Spherical membrane model of bladder

We model the bladder as a two-layered nonlinear elastic spherical membrane subject to an internal pressure p. The governing equation for mechanical equilibrium is:

$$p = \frac{2H_0}{R_0\lambda^3}\left(r_{LP}^H\sigma_{c,LP} + r_{DSM}^H(\sigma_e + \sigma_{c,DSM} + \sigma_m^{act}) + r_{ADV}^H\sigma_{c,ADV}\right) \tag{27}$$

where r_L^H denotes the ratio of the thickness of layer L to total wall thickness H_0 where $L = LP, DSM, ADV$. σ_e denotes the Cauchy stress of elastin, σ_{c_L} denotes the Cauchy stress of collagen in layer L and σ_m^{act} denotes the active Cauchy stress of smooth muscle; H_0 and R_0 denotes the thickness and radius at the unloaded state, and λ denotes the tissue stretch with reference to the unloaded state κ_0.

Parameter	Meaning	Value
k_e	elastin material parameter	$1.15e^3$ Pa
$k_{LP,c}$	collagen material parameters	$6.4e^6$ Pa
$k_{DSM,c}$	layer L (L=LP,DSM,ADV)	$1.6e^6$ Pa
$k_{ADV,c}$		$6.4e^6$ Pa
λ^{att}_{LPc}	min/mode/max	0.75, 0.775, 0.9
λ^{att}_{DSMc}	collagen attachment stretches	0.775, 0.95, 0.975
λ^{att}_{ADVc}	layer L (L=LP,DSM,ADV)	0.6, 0.7, 0.8
k^{act}_m	SMC active modulus	6212 Pa
λ^{min}_m	SMC active stress parameter	0.25
λ^{max}_m	SMC active stress parameter	2.5
λ^{att}_m	SMC attachment stretch	1.6
P^{SHAM}_c	cutoff pressure SHAM	380 Pa
P^{BOO}_c	cutoff pressure BOO	6300 Pa
α_{SHAM}	urethral resistance SHAM	28570Pa/(ml/s)
α_{BOO}	urethral resistance BOO	52630Pa/(ml/s)
Q_{in}	bladder filling rate	$0.8ml$/day
α_c	collagen remodeling rate	7.5
α_m	muscle remodeling rate	7.5
β_m	muscle growth rate	4

Table 4: Default model parameters.

2.5.2. Set-up initial configuration: Geometry; material parameters; G&R parameter

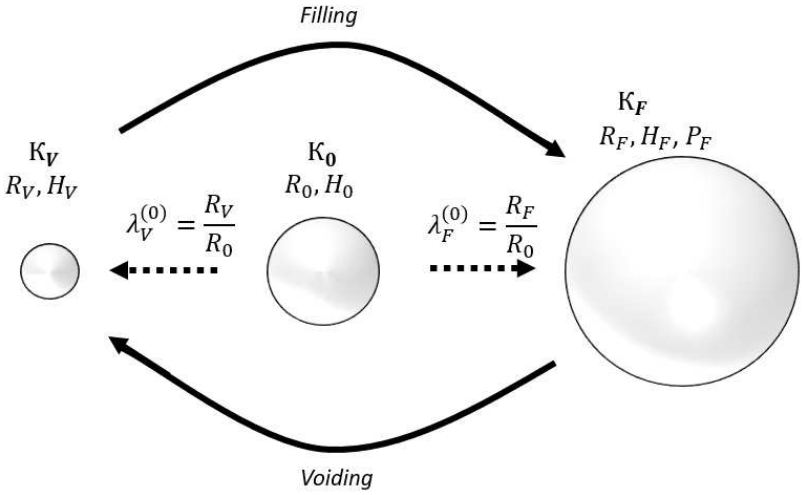

Figure 7: Schematic of different states encountered during cytometry study. κ_0, κ_F and κ_V represent the unloaded, filled and voided states of the bladder, respectively. R_S, H_S, P_S represents the radius, thickness, and pressure at the corresponding state ($S = 0, F, V$). $\lambda_F^{(0)}$ and $\lambda_V^{(0)}$ denote the bladder stretch in the filled and voided configurations.

Geometric, mechanical, urodynamic features of the *in silico* model are informed from experimental measurements (see Tables 1, 2 and 3). At the onset of voiding, the bladder has a radius of 5.8 mm and a wall thickness of 0.21mm. The passive pressure within the bladder at the onset of voiding is 300Pa and the pressure increases to 3800Pa as the SMC generates active force. Voiding takes 12s during which 0.8ml is voided leaving a residual volume of 0.02ml. The modelling steps to set-up the *in silico* model of the the healthy bladder are as follows:

- The radii of the unloaded, voided and filled states, R_0, R_V and R_F

were computed by assuming the bladder to be a hollow sphere. The unloaded spherical radius is $R_0 = (\frac{3V_0}{4\pi})^{1/3}$ where V_0 is the volume of the unloaded bladder which is assumed to be an ellipsoid. Similarly, the bladder radii at voided state κ_v and filled state κ_F (Fig. 7) were calculated by approximating the bladder as a spherical membrane, i.e. $R_F = (\frac{3V_F}{4\pi})^{1/3}$ and $R_v = (\frac{3V_v}{4\pi})^{1/3}$ where V_F and V_v are the filled and voided volumes, respectively.

- The tissue stretches at filled and voided configurations are $\lambda_F = R_F/R_0$ and $\lambda_V = R_V/R_0$, respectively.

- The three recruitment parameters of the collagen triangular recruitment distribution are determined from the collagen attachment stretch distribution parameters (see Fig.8 and Table 4) and the tissue stretch at the filled state (λ_F).

- The initial value of the muscle recruitment stretch is determined by dividing the tissue stretch at filled state λ_F by the muscle attachment stretch λ_m^{at}, i.e. $\lambda_M^R = \lambda_F/\lambda_m^{at}$.

- We observed that collagen was not bearing load at the onset of voiding and hence acts as a protective-sheath against overdistension. Therefore k_E was computed based on the force balance at the initial maximum passive state (R_F) and assumption that only elastin is load bearing. Specifically $K_E = P_{max}^{passive} \frac{R_0 \lambda_F^7}{2H_0 r_{DSM}^H (\lambda_F^6 - 1)}$.

- Collagen material parameters ($k_{LP,c}, k_{DSM,c}, k_{ADV,c}$) are determined by fitting the passive model to the mechanical loading data.

- In the pressure-flow experiment, we measured the maximum passive filling pressure $P_{max}^{passive}$ and maximum voiding pressure $P_{max}^{voiding}$. The difference between these two is the maximum active pressure P_{max}^{act}. From the active force balance equation, we can determined k_m^{act} analytically from $P_{max}^{act} = k_m^{act} \frac{2H_0 r_{DSM}^H}{R_0(\lambda_m^r \lambda_m^{at})^3}(\lambda_m^{at})^4(\lambda_m^{at} - \lambda_m^{min})(\lambda_m^{max} - \lambda_m^{at})$.

- The urethral resistance parameters, P_C and P_C^{BOO}, are determined as follows. At the tissue voided stretch λ_V, the flow-rate $Q(t) = 0$. Hence from eqn.14, we obtain $P_c = P^{act}(\lambda_m(\lambda_V, \lambda_M^R)) - P_C = 0$ where P^{act} is the active pressure (and similarly for P_C^{BOO}). The slope of urethral resistance relationship, α, is then determined by matching the voiding duration of the SHAM bladder; we assume α is a constant and does not adapt during BOO remodelling.

- The collagen remodeling rate α_c and muscle growth rate β_m are numerically determined so that the final void radius matches the experimental void radius and smooth muscle hypertrophy stabilises after around 2 weeks.

2.5.3. Algorithmic workflow

The model is implemented into Matlab and uses two timescales: a longer time-scale τ (days/weeks) for G&R; a short-time scale t (seconds) for computation of urodynamics during voiding; parameter values are detailed in Table.4.

The bladder model is subject to a constant inflow rate. To facilitate visual illustration of the model behaviour, we set the inflow to be 0.8ml/day so that the healthy bladder fills and voids once per day. At each time step, as the

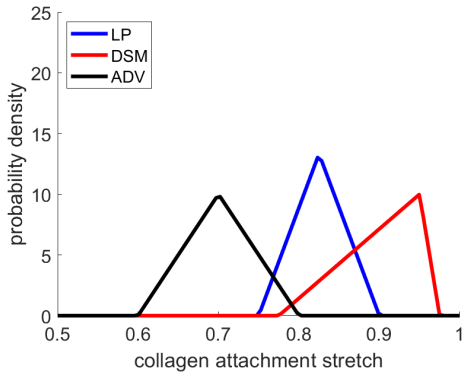

Figure 8: Collagen attachment stretch distributions in the lamina propria, detrusor and adventitial layers.

bladder fills, the updated volume (and radius) of the bladder is computed. The bladder continues to fill until either: voiding is triggered or of it is unable to void, it leaks. If voiding is triggered, urodynamic metrics are computed, the bladder is emptied and the cycle of filling begins again.

- For $\tau < 0$, the bladder can functionally void and is in a homeostatic state.

- To simulate the creation of outlet obstruction, parameters of the pressure-flow relationship (see eqn. 14) are instantaneously changed at $\tau = 0$: the cutoff pressure is increased from P_c^{SHAM} to P_c^{BOO} and the resistance parameter is increased from α_{SHAM} to α_{BOO}.

- Throughout the simulation, maximum stretches of all constituents are computed during voiding cycle (or in the leaky state). These are used to drive remodelling of collagen and SMC recruitment stretches to maintain a homeostatic state about the voiding configuration (see eqns. 17,

19, 18 and 21). Voiding metrics are used to control SMC growth using eqns. 22 or 23 or 24

- Growth and remodelling continues until a new homeostasis is achieved and voiding functionality of bladder restored.

2.5.4. Simulations

In Section 3, we illustrative the *in silico* model of the bladder and it's adaptive response to BOO. We then investigate how the SMC growth rate parameter influences model behaviour and examine several mechanisms to drive SMC growth. Lastly, we compare of model predictions with experiment at 4 weeks post-BOO.

3. Results

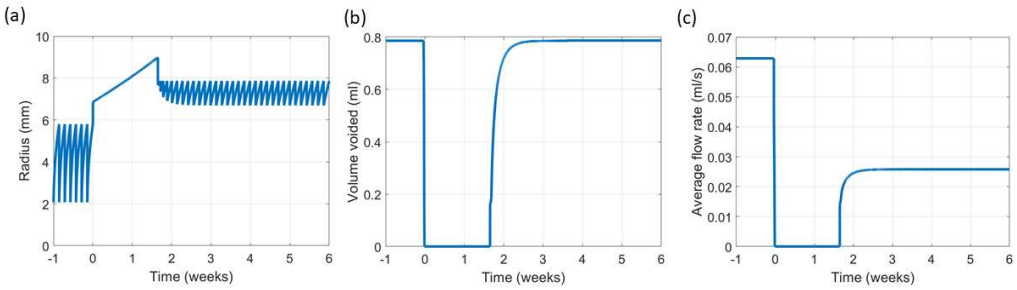

Figure 9: Bladder adaption from pre-obstruction ($t < 0$) to post-obstruction ($t > 0$). (a) Evolution of radius with illustrative filling and voiding cycles. Temporal evolution of (b) volume voided and (c) average flow rate.

Figure 9 overviews the voiding behaviour of the *in silico* bladder, prior to, and in response to outlet obstruction. Note that in this illustrative simulation, the bladder is subject a constant inflow rate of 0.8ml/day and conse-

quently, during the pre-obstruction period ($t < 0$), the healthy bladder voids once per day: the radius varies from around 2mm to 6mm during voiding cycles (see Fig. 9(a)); voiding of 0.8ml/s takes 12 seconds; the peak flow rate is 0.12 ml/s and the average flow rate is 0.06 ml/s. Following obstruction, the bladder is unable to actively void and consequently continues to fill and enlarge. The increase in size is accompanied by a significant increase in the passive pressure as collagen is recruited to load bearing. When the passive pressure becomes sufficiently large, it overcomes the outlet resistance and the bladder begins to leak (*leaky bladder*). The passive pressure continues to increase until the outflow rate matches the filling rate.

During the *leaky bladder* phase, the SMC does not generate sufficient force to contract the bladder and thus the (active) volume voided is zero (see Fig.9b). Between $0 < t < 1.5$ weekns, the leaky bladder increases in size to around 8.5mm as the collagen (which acts as a protective sheath for the healthy bladder) remodels. Once the bladder is able to void again, the maximum stretches of collagen during the voiding cycle reduce below 1 and collagen reverts to being a protective sheath (see Fig. 10). Note that as the bladder enlarges, the collagen recruitment stretch distributions remodel (see Fig. 11) to maintain the collagen stretch distribution towards the attachment stretch distribution at the onset of voiding.

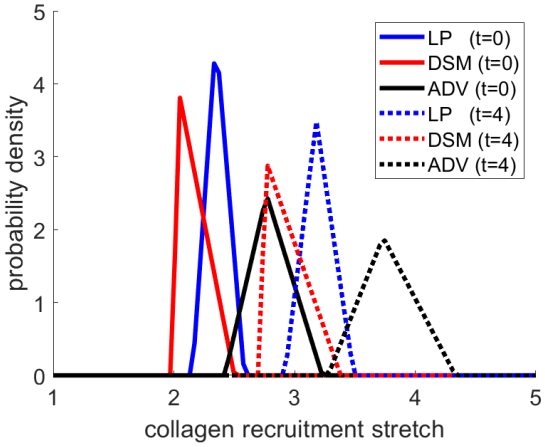

Figure 11: Recruitment stretch distributions in the layers of the bladder for the SHAM bladder ($(t = 0)$ and following G&R in response to BOO.

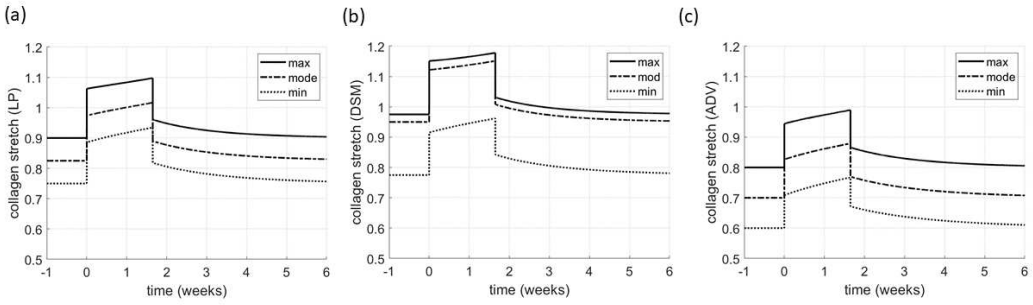

Figure 10: Evolution of collagen stretch distribution (maximum, mode and minimum) for individual layers: (a) lamina propria (b) detrusor and (c) adventitia.

Hypertropy of SMC occurs rapidly during the *leaky bladder* phase (Fig.12). In the model, functional voiding is restored when SMC can generate sufficient force to generate a contraction of the bladder so that the voided SMC stretch is less than the homeostatic SMC voiding stretch ($\lambda_m^{att} = 1.6$). After around 1.5 weeks, the bladder starts to (actively) void again with a small volume and

high frequency. As SMC hypertropy increases, the contractile range of SMC during voiding increases and thus the volume voided increases whilst the voiding frequency decreases. After 3 weeks, the total volume voided is fully restored but the average flow rate is only about 50% of the normal bladder (see Fig.9b,c). Interestingly, due to an increase in size, the post-obstructed bladder can void the same amount of urine as the pre-obstructed bladder with a smaller range of contraction (see Figs. 9a and 13).

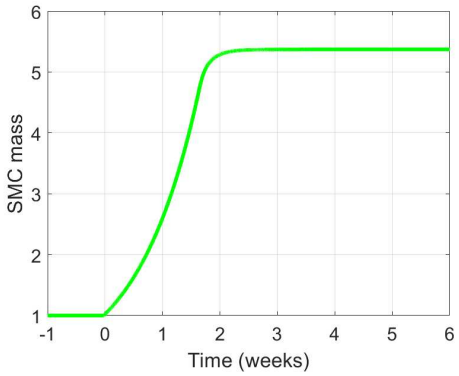

Figure 12: The change of SMC mass during BOO growth and remodeling

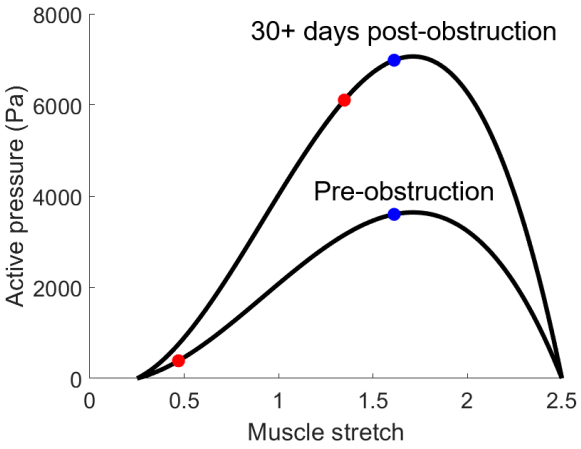

Figure 13: The relation between muscle stretch and active pressure for pre and 30+ days post obstruction. The blue dots showed the onset of voiding and red dots showed the end of voiding

3.1. Bladder urodynamics pre and post obstruction

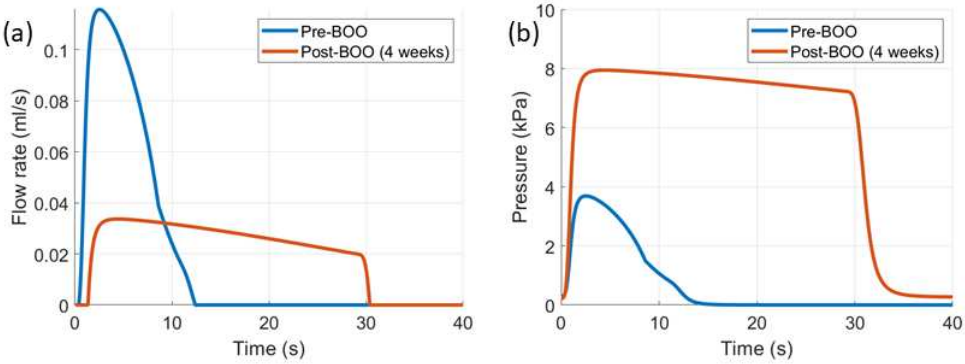

Figure 14: The urodynamic curves of selected time points including (a) time vs. flow rate curve and (b) time vs. pressure curve

From Figure. 14a, it can be seen that the maximum flow rate of the bladder decreases by approximately 75% and the voiding duration more than

doubles. The maximum voiding pressure doubles during voiding for the BOO bladder (see Fig. 14b) due to the SMC hypertrophy.

3.2. Comparison of different growth hypotheses

Three illustrate mechanisms to drive SMC hypertrophy were investigated, restoration of: volume voided; 2. average voiding flow-rate; 3. contractile range. For all cases, the bladder maximum radius was increase by 33 % (see Fig.15) following obstruction. It can be seen that if the bladder adapts to restore average flow rate or contractile range then the volume voided increases (Fig. 16(b)). However, significant increases in SMC mass are required to maintain the contractile range (Fig. 16(a)) and it takes a longer time to achieve homeostasis.

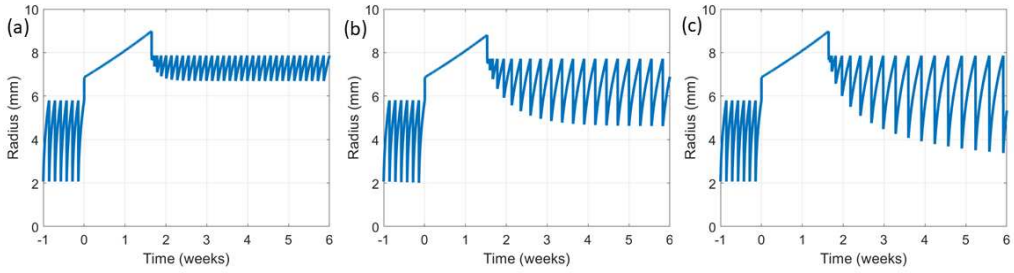

Figure 15: The simulated time vs. radius with different hypothesis of SMC growth (a) SMC growth driven by voided volume driven (b) SMC growth driven by average flow rate (c) SMC growth driven by SMC contraction range

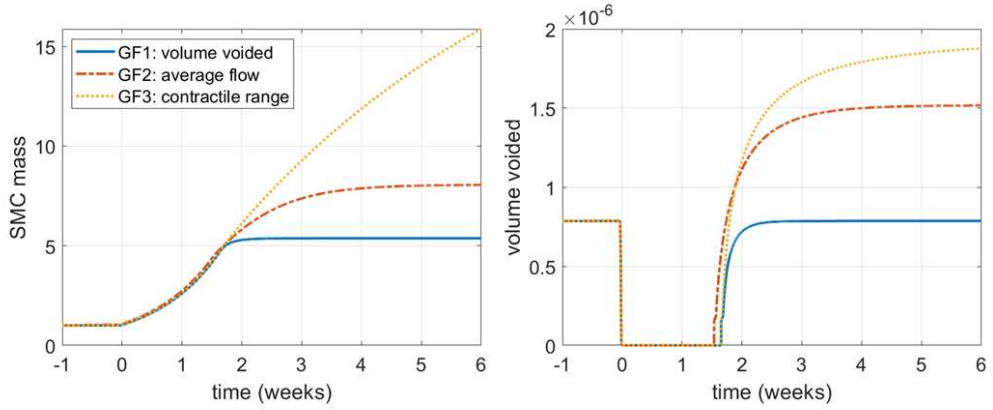

Figure 16: The time vs. (a) SMC mass and (b) volume voided using different SMC growth evolution functions: GF1 (blue) - SMC hypertrophy acts to restore volume voided; GF2 - (red) SMC hypertrophy acts to restore average flow rate; GF3 - (yellow) SMC hypertrophy acts to restore contractile range

3.3. Comparison between simulation and experiment

We conclude the results section by comparing predictions of the *in silico* bladder model with experimental observations. Figure 18 illustrates the rightward shift of the stress-stretch curves for (a) the experimental model and (b) the *in silico* model. Note for comparison with the experimental model, the BOO mechanical response has been plotted relative to the SHAM reference configuration. Figure 17 depicts relevant bladder metrics pre-BOO and 4 weeks post-BOO. It can be seen that there is consistency between model predictions and experiment observations, i.e. the *in silico* bladder: enlarges in size and the wall thickens; voiding volume is conserved whilst the residual volume increases; voiding duration increases; a reduction in the passive filling pressure occurs whilst the maximum void pressure approximately doubles. In fact, quantitative consistency is achieved for most quantities; however, the *in*

492 *silico model* underestimates the increase in wall thickness and void duration.

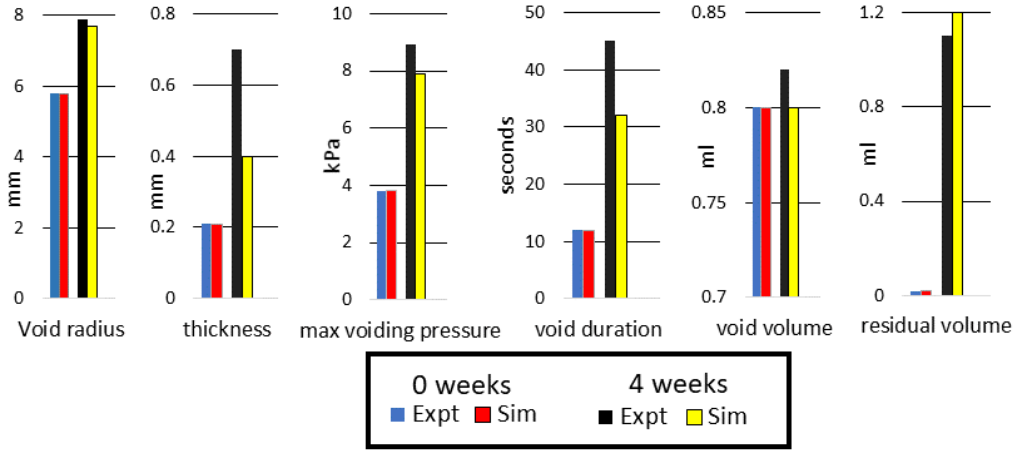

Figure 17: Comparison between *in silico* and experimental model bladder parameters at 4 weeks post-BOO.

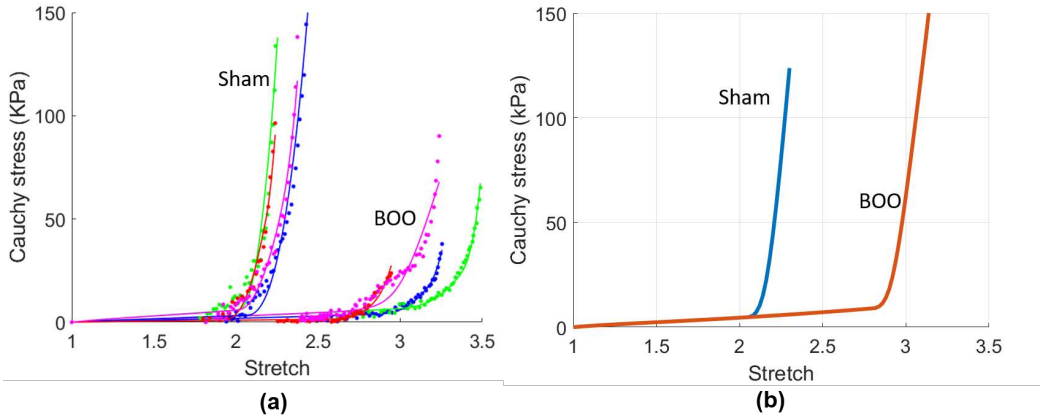

Figure 18: The comparison between (a) experimentally measured mechanical loading curves of SHAM (n=4) and 4 week BOO (n=4) and (b) simulated passive mechanical loading curves of SHAM and 4 week BOO. Note for the comparison, the experimentally measured stretch of BOO bladder is defined relative to the unloaded state κ_0 of SHAM bladder by multiplying the stretch by the ratio of unloaded radii ($R_{0,BOO}/R_{0,Sham}$).

4. Discussion

We have presented the first G&R model of the urinary bladder and used it to simulate the response of the bladder to outlet obstruction. The model provides a mechanistic understanding of how the bladder wall adapts in response to BOO to restore voiding functionality. An integrative *in-vivo in-vitro in-silico* modelling approach underpins the work and enables calibration of the healthy bladder model and informs remodelling assumptions. Consistent with experimental observations in a rat model of BOO, the model predicts that following initiation of BOO, the bladder enters a leaky state after which hypertrophy of SMC restores the ability to void. Moreover, the model correctly predicts that whilst volume voiding is restored by this G&R response,

residual volume increases, the average voiding flow rate decreases and the voiding duration increases. Although the model has good consistency with experiment, it has several limitation, that are discussed below.

Experimental data confirms the bladder undergoes three stages of remodelling in response to BOO: an initial *hypertrophy* phase, followed by a *compensation* phase, and finally, a *decompensation* phase [29]. The hypertrophy stage consists of SMC growth accompanied by angiogenesis to meet the increased metabolic demands of the tissue. During the compensation stage, the bladder maintains effective voiding function but is subject to cyclic ischaemia-reperfusion injury; this leads leads to matrix accumulation (fibrosis) and also neuronal loss [44] that is accompanied diminished SMC contractility. Finally, in the decompensation stage, SMC atrophy occurs leading to loss of bladder functionality. In the present work, we only model the hypertrophy and early compensation stages of BOO- without ischaemic damage. Our integrative *in-vivo in-vitro in-silico* modelling approach provides foundations for developing a more complete representation of all stages of BOO. We envisage such a model may assist in designing/evaluating pharmacological or surgical interventional strategies for clinical management of the disease.

While numerous studies have investigated the relationship between mechanical stimuli and SMC remodeling in arteries as well as the associated set points for homeostasis, very little is known about this type of coupling in the bladder wall. Here, we used the G&R model to investigate hypotheses linking SMC growth to bladder biometrics (volume voided, average voiding flow rate,

contractile range). The first hypothesis we investigated is that the growth of SMC is driven by volume voided. This is based on our experimental observations that volume voided was restored following hypertrophy. Interestingly, others have also observed the bladder to increase in size with higher residual volume whilst maintaining volume voided [45]. However, whilst it is known that mechanical stress can activate signals that mediate bladder wall hypertrophy, the mechanobiological mechanisms that would enable the bladder to sense how much volume it has voided (to drive SMC growth) remain an open question. We also evaluated the hypotheses that SMC growth evolves to restore either average voiding flow rate or SMC contractile range. However, both these hypotheses led to larger increases in volume voided than observed in experiment. We therefore enlisted the first hypothesis for much of the present work. Nevertheless, we conjecture that flow or SMC stretch sensors may be relevant for adaption in non-pathological conditions, e.g. bladder enlargement during development.

Consistent with experiments, the in silico bladder was unable to void following the increase in outlet resistance, resulting in overflow incontinence after which voiding was recovered. Simulations with the G&R model enabled a mechanistic understanding of how this recovery was achieved. Imposition of BOO stimulates rapid SMC hypertrophy. In time, SMC growth is sufficient to generate adequate intravesical pressures to overcome the increased outlet resistance. However, initially, the remodeled bladder voids smaller volumes at higher frequency, compared with the normal bladder. Subsequently, the bladder transitions to the compensated phase as smooth muscle growth

stabilises in response to recovery of voiding function; by design, this model restored volume voided. Consistent with experiments, the model predicted increased void duration following imposition of BOO. However, the predicted increase in void duration was greater than in experiments: 12s to 32s in *in silico* model whilst in the rat model it increased from 12s to 45s. This difference may be attributed to the modelling idealization that neither the stimulus function $S(t)$ nor the functional form of the active stress-stretch relationship are changed in response to BOO. Experimental guidance is needed to gain greater insight into the evolving functionality of SMC so the model can be sophisticated to more accurately simulate the bladder's evolving structural-functional relationship in response to BOO.

We modelled the bladder as a 1D non-linear elastic incompressible, homogeneous spherical membrane. However, the real bladder is not spherical and has spatially heterogenous material properties[46, 21]. Future developments of the model will build on existing computational growth models that account for anatomical geometries[36]; anisotropic volumetric growth [47]; and incorporation of regulatory fibrotic pathways [35]. Consideration of the molecular aspects of the remodelling, (for example, those associated with ischaemia) during the compensation, decompensation stages of BOO will provide insights on the reversibility of pathological changes associated with BOO.

The clinical diagnosis of BOO in the context of a non-neurogenic history, involves taking a detailed urological history and assessing the lower urinary tract symptoms including storage, voiding and post-voiding symptoms. A

variety of symptom score questionnaires are available [10] including the International Prostate Symptom Score, the International Consultation on Incontinence questionnaire, and the Danish Prostate Symptom Score. There is strong evidence that a validated symptom score questionnaire should be used. More generally, the mainstay of assessment of lower urinary tract symptoms (LUTS) is the use of a bladder diary to assess frequency of voiding and the volumes of urine produced, ideally recorded over a consecutive three-day period. Following a clinical examination and analysis of the urine, the use of a blood test to exclude cancer (prostate specific antigen), a post-voiding residual to check that the bladder is emptying to completion and where appropriate a flow test to assess the flow of urine from the bladder through the urethra. In this work, we used our silico model to understand the cause of changes to clinical parameters such as residual volume and voided volume during the G&R response to BOO. In the future, simulations of this kind could be extended to other types of data available in clinical evaluations in order to more directly impact clinical practice.

The animal model of BOO induced by partial urethral ligation has most commonly been used to investigate the pathophysiology of male LUTS associated with BOO resulted from BPH. However, the majority of previous basic research studies on BOO have utilized female animals. Therefore, this project used male rats to produce the BOO condition underlying male LUTS [48]. A recent study also reported that this male BOO model exhibits the early hypertrophy-compensation phase followed by the later decompensation phase of bladder dysfunction, similar to those observed in human BPH/BOO[49].

Animal models may also provide the critical data needed to overcome limitations in current diagnosis and treatment practices. For example, a pressure flow analysis is the conventional approach for diagnosing and defining the severity of BOO in patients who have a complex situations such as failure to respond to initial therapy, existence of significant post-voiding bladder residual, or prior to surgery. Whilst this test has been considered the "gold standard" evaluation for BOO and is used as a predictor of outcome to any surgical intervention to relieve the outlet obstruction, recent work in a randomised study looking at the role of urodynamics prior to surgery raised concerns over this previously widely held opinion[50]. We conjecture that a more mechanistic understanding of the relationship between the urodynamic data and progressive changes to the bladder wall during the three stages of BOO pathology is essential for addressing these limitations. Such an understanding requires a modelling approach of the kind developed here that integrates a model of filling/voiding with a longer time scale G&R model. Moreover, we envisage future work that leverages the *in vivo in vitro in silico* approach introduced here will enable the design of new diagnostic tools for assessing bladder dysfunction and provide guidance on developing new treatments.

5. Conclusion

We present a novel model for the bladder's adaptive G&R response to outlet obstruction. Predictions of the model were consistent with *in vivo* experiments of bladder outlet obstruction. This work is an important step towards the development of patient specific *in silico* models of the bladder that can predict changes to bladder functionality and hence guide the selection and timing of patient treatment. We envisage these models can be leveraged in the future so clinicians can make more effective use of diagnostic data and researchers can design new pharmacological and surgical interventions.

6. Acknowledgements

Paul Watton acknowledges partial support towards this work from UK EPSRC (EP/N014642/1).

References

[1] I.C. Society, ICS Standards 2020-2021, 2021.

[2] N. D. Patel, J. K. Parsons, Age and bladder outlet obstruction are independently associated with detrusor overactivity in patients with benign prostatic hyperplasia., European urology 54(2) (2008) 419–426.

[3] N. D. Patel, J. K. Parsons, Epidemiology and etiology of benign prostatic hyperplasia and bladder outlet obstruction., Indian journal of urology 30.2 (2014) 170.

[4] S. K. Reddy, A. B. Shaik, Non-invasive evaluation of bladder outlet obstruction in benign prostatic hyperplasia: a clinical correlation study., Arab journal of urology 17(4) (2019) 259–264.

[5] A. Groutz, J. G. Blaivas, D. C. Chaikin, Bladder outlet obstruction in women: definition and characteristics, Neurourology and Urodynamics: Official Journal of the International Continence Society 19 (2000) 213–220.

[6] S. Tritschler, A. Roosen, C. Füllhase, C. G. Stief, H. Rübben, Urethral stricture: etiology, investigation and treatments, Deutsches Ärzteblatt International 110 (2013) 220.

[7] A. Alwaal, S. D. Blaschko, J. W. McAninch, B. N. Breyer, Epidemiology of urethral strictures, Translational andrology and urology 3(2) (2019) 209.

[8] K. B. Egan, The epidemiology of benign prostatic hyperplasia associated with lower urinary tract symptoms: prevalence and incident rates, Urologic Clinics 43 (2016) 289–297.

[9] V. W. Nitti, Pressure flow urodynamic studies: the gold standard for diagnosing bladder outlet obstruction, Reviews in urology 7 (2005) S14.

[10] https://uroweb.org/guideline/treatment-of-non-neurogenic-male-luts (????).

[11] D. A. Taub, J. T. Wei, The economics of benign prostatic hyperplasia and lower urinary tract symptoms in the united states, Current Prostate Reports 4 (2006) 81–90.

[12] F. Cheng, L. A. Birder, F. A. Kullmann, J. Hornsby, P. N. Watton, S. Watkins, M. Thompson, A. M. Robertson, Layer-dependent role of collagen recruitment during loading of the rat bladder wall, Biomechanics and Modeling in Mechanobiology 17 (2018) 403–417.

[13] J. G. Susset, C. H. Regnier, Viscoelastic properties of bladder strips: standardization of a technique., Investigative urology 18 (1981) 445–450.

[14] M. Coldinq-Jørqensen, K. Steven, A model of the mechanics of smooth muscle reservoirs applied to the intestinal bladder, Neurourology and Urodynamics 12 (1993) 59–79.

[15] U. Hübener, R. Van Mastrigt, Computer simulation of micturition, Urodinamica 4 (1994) 81–90.

[16] A. J. Van Beek, A finite element model of the urinary bladder (1997).

[17] S. Wognum, D. E. Schmidt, M. S. Sacks, On the mechanical role of de novo synthesized elastin in the urinary bladder wall, Journal of biomechanical engineering 131 (2009) 101018.

[18] A. N. Natali, A. L. Audenino, W. Artibani, C. G. Fontanella, E. L. Carniel, E. M. Zanetti, Bladder tissue biomechanical behavior: Experimental tests and constitutive formulation, Journal of Biomechanics 48 (2015) 3088–3096.

[19] J. Hornsby, D. M. Daly, D. Grundy, F. Cheng, A. M. Robertson, P. N. Watton, M. S. Thompson, Quantitative multiphoton microscopy of murine urinary bladder morphology during in situ uniaxial loading, Acta Biomaterialia 64 (2017) 59–66.

693 [20] M. Borsdorf, A. Tomalka, N. Stutzig, E. Morales-Orcajo, M. Böl,
694 T. Siebert, Locational and directional dependencies of smooth mus-
695 cle properties in pig urinary bladder, Frontiers in physiology 10 (2019)
696 63.

697 [21] R. Trostorf, E. Morales-Orcajo, T. Siebert, M. Böl, Location-and layer-
698 dependent biomechanical and microstructural characterisation of the
699 porcine urinary bladder wall, journal of the mechanical behavior of
700 biomedical materials 115 (2021) 104275.

701 [22] D. J. Griffiths, H. J. Rollema, Urine flow curves of healthy males: a
702 mathematical model of bladder and urethal function during micturition,
703 Medical & Biological Engineering & Computing 17 (1979) 291–300.

704 [23] M. S. Damaser, S. L. Lehman, Two mathematical models explain the
705 variation in cystometrograms of obstructed urinary bladders, Journal of
706 biomechanics 29 (1996) 1615–1619.

707 [24] F. A. Valentini, G. R. Besson, P. P. Nelson, P. E. Zimmern, A math-
708 ematical micturition model to restore simple flow recordings in healthy
709 and symptomatic individuals and enhance uroflow interpretation, Neu-
710 rourology and Urodynamics: Official Journal of the International Con-
711 tinence Society 19 (2000) 153–176.

712 [25] A. Pigne, F. A. Valentini, P. P. Nelson, Comparison at short follow-up
713 of the changes in the voiding phase induced by sub-urethral tapes using
714 a mathematical micturition model, Current Urology 3 (2009) 179–184.

715 [26] W. Fletcher, A computer simulation of micturition (2005) 1–36.

[27] R. Seydewitz, R. Menzel, T. Siebert, M. Böl, Three-dimensional mechano-electrochemical model for smooth muscle contraction of the urinary bladde, J Mech Behav Biomed Mater 75 (2017) 128–14.

[28] F. Cheng, P. N. Watton, et al., An integrative biomechanics-micturition model of the urinary bladder, to be submitted (2021).

[29] F. Fusco, M. Creta, C. De Nunzio, V. Iacovelli, F. Mangiapia, V. L. Marzi, E. F. Agrò, Progressive bladder remodeling due to bladder outlet obstruction: a systematic review of morphological and molecular evidences in humans, BMC urology 18 (2018) 1–11.

[30] E.-i. Takaoka, M. Kurobe, H. Okada, S. Takai, T. Suzuki, N. Shimizu, J. Kwon, H. Nishiyama, N. Yoshimura, C. J. Chermansky, Effect of trpv4 activation in a rat model of detrusor underactivity induced by bilateral pelvic nerve crush injury, Neurourology and urodynamics 37 (2018) 2527–2534.

[31] J. Nishiguchi, D. D. Kwon, Y. Kaiho, M. B. Chancellor, H. Kumon, P. B. Snyder, N. Yoshimura, Suppression of detrusor overactivity in rats with bladder outlet obstruction by a type 4 phosphodiesterase inhibitor, BJU international 99 (2007) 680–686.

[32] P. N. Watton, Y. Ventikos, G. A. Holzapfel, Modelling the mechanical response of elastin for arterial tissue, Journal of Biomechanics 42 (2009) 1320–1325.

[33] M. R. Hill, X. Duan, G. A. Gibson, S. Watkins, R. A. M., A theoretical and non-destructive experimental approach for direct inclusion of

measured collagen orientation and recruitment into mechanical models of the artery wall, Journal of biomechanics 45 (2012) 762–71.

[34] P. Watton, N. Hill, M. Heil, A mathematical model for the growth of the abdominal aortic aneurysm, Biomechanics and modeling in mechanobiology 3 (2004) 98–113.

[35] P. Aparício, M. S. Thompson, P. N. Watton, A novel chemo-mechano-biological model of arterial tissue growth and remodelling, Journal of Biomechanics 49 (2016) 2321–2330.

[36] F. S. Teixeira, E. Neufeld, N. Kuster, P. N. Watton, Modeling intracranial aneurysm stability and growth: an integrative mechanobiological framework for clinical cases, Biomechanics and modeling in mechanobiology 19 (2020) 2413–2431.

[37] H. Chen, Intracranial aneurysm disease: novel modelling of inception and the microstructural adaption of collagen fabric, Ph.D. thesis, Department of Engineering Science, University of Oxford, 2014.

[38] P. Bhogal, G. Pederzani, A. Grytsan, Y. Loh, P. A. Brouwer, T. Andersson, N. Gundiah, A. M. Robertson, P. N. Watton, M. Söderman, The unexplained success of stentplasty vasospasm treatment : Insights using mechanistic mathematical modeling, Clinical Neuroradiology 29 (2019) 763–774.

[39] J. Le Feber, E. Van Asselt, R. Van Mastrigt, Neurophysiological modeling of voiding in rats: bladder pressure and postganglionic bladder nerve activity, The American journal of physiology 272 (1997) R413–R421.

[40] B. Uvelius, Length-tension relations of in vitro urinary bladder smooth muscle strips, Journal of Pharmacological and Toxicological Methods 45 (2001) 87–90.

[41] D. J. Griffiths, The mechanics of the urethra and of micturition, British Journal of Urology 45 (1973) 497–507.

[42] C. P. Bates, E. P. Arnold, D. J. Griffiths, The nature of the abnormality in bladder neck obstruction, British Journal of Urology 47 (1975) 651–656.

[43] L. A. Birder, S. de Wachter, J. Gillespie, J. J. Wyndaele, Urethral sensation: basic mechanisms and clinical expressions, International Journal of Urology 21 (2014) 13–16.

[44] R. Levin, P. Chichester, S. Levin, R. Buttyan, Role of angiogenesis in bladder response to partial outlet obstruction, Scandinavian Journal of Urology and Nephrology 38 (2004) 37–47.

[45] V. W. Nitti, L. M. Tu, J. Gitlin, Diagnosing bladder outlet obstruction in women, The Journal of urology 161 (1999) 1535–1540.

[46] E. Morales-Orcajo, T. Siebert, M. Böl, Location-dependent correlation between tissue structure and the mechanical behaviour of the urinary bladder, Acta biomaterialia 75 (2018) 263–278.

[47] A. Grytsan, T. S. E. Eriksson, P. N. Watton, T. C. Gasser, Growth description for vessel wall adaptation: A thick-walled mixture model of abdominal aortic aneurysm evolution, Materials 10 (2017) 994.

[48] P. Zvara, J. Kliment Jr, A. L. DeRoss, B. H. Irwin, S. E. Malley, M. K. Plante, M. A. Vizzard, Differential expression of bladder neurotrophic factor mrna in male and female rats after bladder outflow obstruction, Journal of Urology 168 (2002) 2682–8.

[49] N. Shinkai, K. Ichihara, K. Kobayashi, H. Tabata, K. Hashimoto, F. Fukuta, T. Tanaka, N. Masumori, Long-term tadalafil administration can prevent functional and structural changes of the urinary bladder in male rats with partial bladder outlet obstruction, Neurourol Urodyn 39 (2020) 1330–1337.

[50] K. Bailey, P. Abrams, P. S. Blair, C. Chapple, C. Glazener, J. Horwood, J. A. Lane, J. McGrath, S. Noble, R. Pickard, G. Taylor, G. J. Young, M. J. Drake, A. L. Lewis, Urodynamics for prostate surgery trial; randomised evaluation of assessment methods (upstream) for diagnosis and management of bladder outlet obstruction in men: study protocol for a randomised controlled trial, Trials 16 (2015) 567.